ChemPubSoc Europe

DOI: 10.1002/chem.201700820

CHEMISTRY
A European Journal
Full Paper

Iron Complexes | *Hot Paper*

Spin States of Homochiral and Heterochiral Isomers of $[Fe(PyBox)_2]^{2+}$ Derivatives

Kay E. Burrows,[a] Sarah E. McGrath,[a] Rafal Kulmaczewski,[a] Oscar Cespedes,[b] Simon A. Barrett,[a] and Malcolm A. Halcrow*[a]

Abstract: The following iron(II) complexes of 2,6-*bis*(oxazolinyl)pyridine (PyBox; L^H) derivatives are reported: $[Fe(L^H)_2][ClO_4]_2$ (**1**); $[Fe((R)\text{-}L^{Me})_2][ClO_4]_2$ ((*R*)-**2**; L^{Me} = 2,6-*bis*{4-methyloxazolinyl}pyridine); $[Fe((R)\text{-}L^{Ph})_2][ClO_4]_2$ ((*R*)-**3**) and $[Fe((R)\text{-}L^{Ph})((S)\text{-}L^{Ph})][ClO_4]_2$ ((*RS*)-**3**; L^{Ph} = 2,6-*bis*{4-phenyloxazolinyl}pyridine); and $[Fe((R)\text{-}L^{iPr})_2][ClO_4]_2$ ((*R*)-**4**) and $[Fe((R)\text{-}L^{iPr})((S)\text{-}L^{iPr})][ClO_4]_2$ ((*RS*)-**4**; L^{iPr} = 2,6-*bis*{4-*iso*propyloxazolinyl}pyridine). Solid (*R*)-**3**·$MeNO_2$ exhibits an unusual very gradual, but discontinuous thermal spin-crossover with an approximate $T_{1/2}$ of 350 K. The discontinuity around 240 K lies well below $T_{1/2}$, and is unconnected to a crystallographic phase change occurring at 170 K. Rather, it can be correlated with a gradual ordering of the ligand conformation as the temperature is raised. The other solid compounds either exhibit spin-crossover above room temperature (**1** and (*RS*)-**3**), or remain high-spin between 5–300 K [(*R*)-**2**, (*R*)-**4** and (*RS*)-**4**]. Homochiral (*R*)-**3** and (*R*)-**4** exhibit more twisted ligand conformations and coordination geometries than their heterochiral isomers, which can be attributed to steric clashes between ligand substituents [(*R*)-**3**]; or, between the isopropyl substituents of one ligand and the backbone of the other ((*R*)-**4**). In solution, (*RS*)-**3** retains its structural integrity but (*RS*)-**4** undergoes significant racemization through ligand redistribution by ^1H NMR. (*R*)-**4** and (*RS*)-**4** remain high-spin in solution, whereas the other compounds all undergo spin-crossover equilibria. Importantly, $T_{1/2}$ for (*R*)-**3** (244 K) is 34 K lower than for (*RS*)-**3** (278 K) in CD_3CN, which is the first demonstration of chiral discrimination between metal ion spin states in a molecular complex.

Introduction

Although the phenomenon of spin-crossover (SCO) was first elucidated over fifty years ago,[1] SCO complexes and molecular materials derived from them continue to be heavily studied.[2–4] On the one hand, control of the temperature and form of an SCO transition is a challenging problem in molecular design and crystal engineering,[5] which impacts areas as diverse as bioinorganic chemistry,[6,7] catalysis[6,8] and solid state physics.[9] On the other hand, SCO compounds have important applications in their own right as multifunctional switches in molecular materials[10,11] and metal–organic frameworks (MOFs),[12] in devices[13] and in nanoscience.[14,15]

One property that has been little explored up to now is the interplay between SCO and chirality, which could in principle lead to switchable non-linear optical (NLO) materials.[16] Many solid SCO materials are adventitiously chiral from crystallizing in polar or handed space groups, and chiroptical switching has indeed been demonstrated in one such compound.[17] Alternatively, chiral materials based on achiral SCO molecules have been prepared through doping them into chiral host frameworks,[18] or crystallizing them with chiral counterions.[19] However, chiral-at-molecule SCO compounds are rare,[20–26] with most studies involving just two series of iron(II) complexes: a family of bidentate Schiff base complexes formed from chiral amines;[20–23] and, a macrocyclic ligand with an asymmetric pattern of backbone substituents.[24,25] The influence of chirality on the SCO properties of such compounds has only recently begun to be investigated and, importantly, all data published thus far have been measured in the solid state.[22,23,25,26] The effect of ligand structure on molecular spin states is better quantified in solution, in which the spin state of a complex is not influenced by lattice effects.[27]

To probe the influence of chirality on SCO, we have turned to the family of 2,6-bis(oxazolinyl)pyridine (PyBox; Scheme 1) heterocyclic ligands,[28] which are suited to this challenge for several reasons. Optically pure substituted PyBox derivatives (L^R, R ≠ H; Scheme 1) are readily available because of their im-

[a] K. E. Burrows, S. E. McGrath, Dr. R. Kulmaczewski, S. A. Barrett, Prof. M. A. Halcrow
School of Chemistry, University of Leeds
Woodhouse Lane, Leeds, LS2 9JT (UK)
Fax: (+44) 113-343-6565
E-mail: m.a.halcrow@leeds.ac.uk
Homepage: http://www.chem.leeds.ac.uk/People/Halcrow.html

[b] Dr. O. Cespedes
School of Physics and Astronomy, University of Leeds
E. C. Stoner Building, Leeds, LS2 9JT (UK)

Supporting information and the ORCID number(s) for the author(s) of this article can be found under https://doi.org/10.1002/chem.201700820. Experimental data can also be obtained from the University of Leeds library at http://doi.org/10.5518/184.

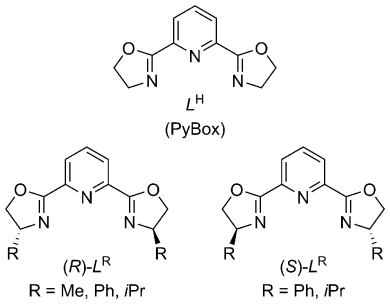

Scheme 1. The ligands employed in this study.

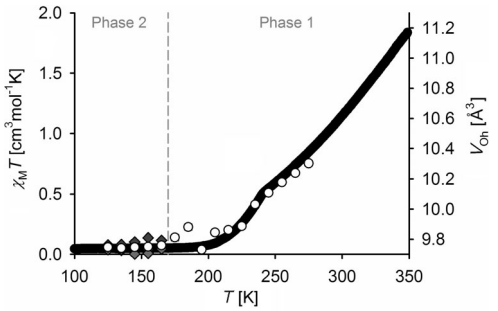

Figure 1. Comparison of the SCO transition in (*R*)-**3**·$MeNO_2$ as monitored by magnetic susceptibility data (black); and, the expansion of the metal-ion coordination sphere as expressed by V_{Oh} (white circles).[41] In Phase 2, the three unique molecules are shown as yellow, red and green diamonds with the white circles representing the average of the three.

portance in asymmetric catalysis,[28,29] and have been used as supporting ligands in other types of chiral molecular magnets.[30] Moreover, the heterochiral isomers $[M((R)\text{-}L^{Ph})((S)\text{-}L^{Ph})]^{2+}$ (Scheme 1; M = Fe,[31] Co,[31,32] Zn[31,33] or another metal ion[31]) have been shown to be stable in solution, without racemization through ligand redistribution reactions. Lastly, the ability of $[Fe(PyBox)_2]^{2+}$ centers to support SCO has been recently demonstrated using achiral PyBox ligands.[34,35] We report here iron complexes of three chiral PyBox derivatives, including a comparison of the spin state properties of the homochiral and heterochiral diastereomers of $[Fe(L^{Ph})_2]^{2+}$ and $[Fe(L^{iPr})_2]^{2+}$ (Scheme 1). We also describe an unusual example of a gradual, but discontinuous, solid state SCO that was discovered during the course of this work.

Results and Discussion

The complexes $[Fe(L^H)_2][ClO_4]_2$ (**1**),[35] $[Fe((R)\text{-}L^{Me})_2][ClO_4]_2$ [(*R*)-**2**], $[Fe((R\text{-}L^{Ph})_2][ClO_4]_2$ [(*R*)-**3**] and $[Fe((R)\text{-}L^{iPr})_2][ClO_4]_2$ [(*R*)-**4**] were prepared by complexing $Fe[ClO_4]_2\cdot 6H_2O$ with 2 equiv of the appropriate L^R ligand in nitromethane or acetonitrile. Heterochiral $[Fe((R)\text{-}L^{Ph})((S)\text{-}L^{Ph})][ClO_4]_2$ [(*RS*)-**3**] and $[Fe((R)\text{-}L^{iPr})((S)\text{-}L^{iPr})][ClO_4]_2$ [(*RS*)-**4**] were similarly obtained, using a 1:1 ratio of the two ligand isomers. All the complexes were dark orange polycrystalline solids following the usual work-up, irrespective of their spin-state properties at room temperature.

The most noteworthy behaviour in the solid state is shown by (*R*)-**3**, which was purified as its nitromethane solvate.[36] Since this lattice solvent is lost upon extended drying in vacuo, all the solid-state measurements described below were performed using freshly prepared and protected crystalline samples to minimize any solvent loss. Bulk samples of (*R*)-**3**·$MeNO_2$ are fully low-spin below 200 K from magnetic susceptibility data, but exhibit a gradual, non-hysteretic thermal spin-crossover at higher temperatures with a $T_{1/2}$ of about 350 K, from its $\chi_M T$ value of 1.8 cm^{3}mol^{-1} K at that temperature (Figure 1). Unusually, there is a clear discontinuity around 240 K in the transition curve, when the sample is about 15% high-spin.[36] Discontinuous SCO transitions are well known and can reflect the presence of multiple independent switching sites in the lattice,[37] a crystallographic phase transition during SCO,[38] or a more subtle order:disorder transition in a ligand or anion.[39] This was probed in (*R*)-**3**·$MeNO_2$ through crystallographic refinements between 125 and 275 K at 10 K intervals, using the same crystal throughout.[40]

Crystalline (*R*)-**3**·$MeNO_2$ undergoes a crystallographic phase change at 170 ± 5 K. The room-temperature phase (Phase 1) adopts the orthorhombic space group $C222_1$ with $Z = 4$. The asymmetric unit of this phase contains half a formula unit, with the complex molecule spanning a crystallographic C_2 axis. Below 170 K, the crystal transforms to Phase 2 through a tripling of the unit cell *b* dimension. Phase 2 has three unique molecules of the complex per asymmetric unit in the space group $P2_12_12_1$ ($Z = 12$). Importantly, however, this phase change is unrelated to the spin-crossover discontinuity, which occurs at 70 K higher temperature (Figure 1). The iron centres in (*R*)-**3**·$MeNO_2$ are fully low spin in both phases near the phase-transition temperature (Table 1).

In Phase 1 at $T \geq 205$ K, refinement models based on an ordered C_2-symmetric half-molecule of the cation gave the best results. This included disorder at one, or both, of the unique phenyl substituents which, unusually, became more severe as the temperature was lowered. Below 235 K, a gradual enlargement and elongation of the displacement ellipsoids was observed, reaching a maximum at 195 K around the temperature at which the molecule becomes fully low-spin (Figure 2). Further cooling from 195 K to the phase transition temperature reversed this trend, with the atomic displacement ellipsoids becoming more regular in shape (Figure 2). This indicates the onset of additional disorder in the complex between 235 K and the phase transition. Between 175–195 K, disorder of the whole molecule about the crystallographic C_2 axis was resolved in the Fourier map, and could be modelled without restraints. Although their residuals are similar, the displacement ellipsoids and metric parameters in the whole-molecule disorder refinement are chemically more reasonable than the C_2-symmetric half-molecule model.[40]

The Phase 2 structures of (*R*)-**3**·$MeNO_2$ between 125 and 165 K are essentially identical, apart from the partial quenching of disorder in the anions, solvent and one phenyl substituent at lower temperatures. The three unique complex molecules in the asymmetric unit remain fully low-spin across this temperature range (Figure 1, Table 1 and Supporting Information[40]).

Notwithstanding some scatter between 175–205 K, the crystallographic and magnetic measurements from (*R*)-**3**·$MeNO_2$ are in excellent agreement (Figure 1).[40] In particular, the crys-

Table 1. Selected bond lengths [Å, Å^3] and angular parameters [deg] in the crystal structures of the complexes in this work. V_{Oh}, Σ and Θ are indices showing the spin state of the complex,[41] whereas ϕ and θ are measures of the angular Jahn–Teller distortion sometimes shown by these iron centers in their high-spin state.[42] Typical values for these parameters in $[Fe(PyBox)_2]^{2+}$ and related complexes are given in refs. [35] and [43]. Data for (*R*)-**3**·$MeNO_2$ at other temperatures are in the Supporting Information.[40]

	(*R*)-**2**[a]	(*R*)-**3**·$MeNO_2$				
T [K]	130	275 (Phase 1)[a]	175 (Phase 1)[a]	125 (Phase 2)[b] Molecule A	Molecule B	Molecule C
Fe–N{pyridyl}	2.137(2)	1.948(4), 1.954(4)	1.908(7), 1.913(9)	1.900(2), 1.906(2)	1.897(2), 1.907(2)	1.902(2), 1.909(2)
Fe–N{oxazolinyl}	2.1883(19), 2.207(2)	2.015(3), 2.052(3)	1.921(18)–2.090(18)	1.975(2)–2.011(2)	1.982(2)–2.009(2)	1.980(2)–2.017(2)
V_{Oh}	12.622(9)	10.303(11)	9.81(2)	9.732(7)	9.762(7)	9.747(7)
Σ	144.0(3)	107.5(4)	100(2)	97.1(3)	92.4(3)	91.2(3)
Θ	448	331	298	292	288	292
ϕ	170.91(11)	180	180	177.75(10)	178.31(10)	179.51(9)
θ	86.50(3)	83.85(6)	84.53(10)	82.45(2)	84.50(2)	86.00(2)

	(*RS*)-**3**·3 MeCN		(*R*)-**4**·$^1/_2$ MeCN[c]		(*RS*)-**4**
T [K]	250	120	120 Molecule A	Molecule B	120
Fe–N{pyridyl}	1.909(2), 1.912(2)	1.9069(18), 1.9108(17)	2.121(3), 2.132(3)	2.117(3), 2.119(3)	2.1170(14), 2.1343(14)
Fe–N{oxazolinyl}	1.980(3)–1.995(2)	1.9793(19)–1.9887(18)	2.210(3)–2.295(3)	2.244(3)-2.276(3)	2.2009(14)–2.2771(15)
V_{Oh}	9.746(8)	9.686(6)	12.866(12)	12.998(12)	12.802(5)
Σ	92.5(4)	91.9(3)	160.4(4)	170.9(4)	142.7(2)
Θ	302	299	452	461	452
ϕ	178.43(11)	178.18(8)	165.50(12)	175.44(11)	163.62(6)
θ	89.14(4)	88.94(2)	70.03(3)	70.32(3)	89.23(1)

[a] The complex cation in this crystal has crystallographic C_2 symmetry, with half a molecule in its asymmetric unit. [b] There are three unique complex molecules in the asymmetric unit of this crystal. [c] There are two unique complex molecules in the asymmetric unit of this crystal.

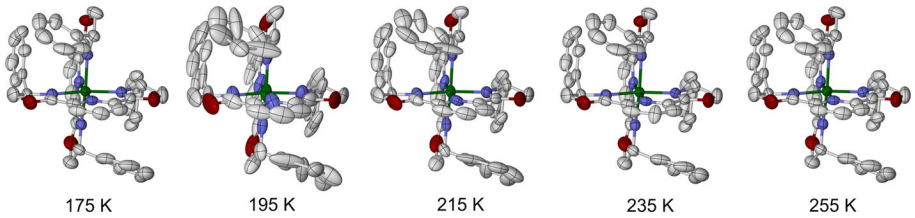

Figure 2. The complex molecule in Phase 1 of (*R*)-**3**·$MeNO_2$ at different temperatures with all atoms modelled as crystallographically ordered, showing the maximum thermal disorder around 195 K. Displacement ellipsoids are at the 50% probability level, and H atoms are omitted. Color code: C, white; Fe, green; N, blue; O, red.

tallographic data reproduce the discontinuity near 240 K. A plot of the unit cell volume of (*R*)-**3**·$MeNO_2$ with temperature also shows an inflection at 220 K, which is associated with a clear decrease in the *c* dimension on cooling from 240–200 K. The unique axes of the C_2-symmetric cations in Phase 1 align along *b*. The meridional ligands extend along the (010) plane, with the most disordered phenyl groups all oriented towards the *c* direction.[40] Thus, the additional decrease in *c* between 240–200 K is consistent with the gradual disordering of the ligand conformations over that temperature range, implied by the atomic displacement ellipsoids (Figure 2). In summary, the SCO discontinuity in (*R*)-**3**·$MeNO_2$ at 240 K is associated with the onset of increased ligand disorder below that temperature. That may reflect a mismatch between the progress of SCO and the thermal contraction of the bulk crystal lattice on cooling below 240 K, until 170 K when the Phase 1→2 transition occurs.

The other new complexes in this work have more routine spin-state behaviour from magnetic susceptibility data. Solid **1** ($T_{1/2} \approx 350$ K)[35] and (*RS*)-**3** ($T_{1/2} > 400$ K) exhibit gradual SCO above room temperature, whereas (*R*)-**2**, (*R*)-**4** and (*RS*)-**4** are all high-spin between 3–300 K. These compounds were all also crystallographically characterized; the spin states of the crystalline compounds, as derived from their metric parameters, are all consistent with the magnetic susceptibility data. The solid compounds each form solvent-free polycrystalline powders upon drying. All these solid materials, including (*RS*)-**3** and (*RS*)-**4**, are phase-pure and isostructural with the single crystalline phases by X-ray powder diffraction.[40]

The complex cations in crystalline (*R*)-**2**, (*R*)-**4**·$^1/_2$ MeCN (which contains two unique molecules per asymmetric unit) and (*RS*)-**4** are high-spin at 120 or 130 K, according to their metric parameters (Table 1). High-spin complexes with this type of ligand geometry are prone to an angular Jahn–Teller distortion towards a trigonal prismatic coordination geometry.[43,44] This is crystallographically quantified by two parameters: the *trans*-N{pyridine}-Fe-N{pyridine} angle (ϕ in Table 1); and the dihedral angle between the least squares planes of

the two ligands (θ in Table 1).[45] High-spin complexes that deviate significantly from the ideal values of $\phi = 180^\circ$ and $\theta = 90^\circ$ rarely exhibit SCO on cooling[46] because the associated structural rearrangement from a distorted high-spin to undistorted low-spin state is inhibited by the surrounding solid lattice.[47] Based on data available from $[Fe(bpp)_2]^{2+}$ derivatives, all the high-spin complexes in this work exhibit values of ϕ or θ that would disfavour [(*R*)-**2**] or prohibit [(*R*)-**4**·$^1/_2$MeCN and (*RS*)-**4**] SCO below room temperature.[35,43,46] Space-filling models reveal no steric contacts involving the methyl substituents in (*R*)-**2** that could influence the metal ion spin-state, by hindering contraction of the Fe–N bonds during SCO for example.[40,48] However, the steric influence of the isopropyl groups in (*R*)-**4** and (*RS*)-**4** may influence the high-spin nature of those compounds (see below). Finally, the solvate (*RS*)-**3**·3MeCN is crystallographically low-spin at 120 and 250 K. As usual for low-spin complexes, the coordination geometries of low-spin (*R*)-**3**·$MeNO_2$ and (*RS*)-**3**·3 MeCN, as expressed by ϕ and θ, are more regular than for the high-spin compounds (Table 1).

Despite their different spin states, the complex cations in (*R*)-**3**·$MeNO_2$ and (*R*)-**4**·$^1/_2$MeCN both exhibit more twisted coordination geometries and ligand conformations than their heterochiral isomers (*RS*)-**3**·3 MeCN and (*RS*)-**4**. This reflects interligand steric clashes between the phenyl or isopropyl substituents in the homochiral isomers, that are not present in the corresponding heterochiral molecules (Figures 2 and 3). The degree of twisting, as measured by the dihedral angle between the least squares planes of their ligands (θ, Table 1), is greater in (*R*)-**4** [$70.03(3) \le \theta \le 70.32(3)^\circ$] than in (*R*)-**3** [$82.45(2) \le \theta \le 86.00(2)^\circ$] at 120–125 K. This reflects the greater steric bulk of the *i*Pr substituents, and the greater conformational flexibility of the high-spin iron centres in (*R*)-**4**.

The other notable difference between the molecular conformations in the solvates of (*R*)-**3** and (*RS*)-**3** is the disposition of their phenyl substituents. In (*RS*)-**3**, both phenyl substituents from one Ph_2PyBox ligand sandwich the phenyl ring from the other ligand, with three of them forming clear inter-ligand π–π interactions to that pyridyl ring in the crystal structure.[40] In (*R*)-**3**, the phenyl substituents of one ligand are roughly co-parallel with the neighbouring pyridyl group, as before, but the phenyl groups of the other ligand are twisted so that one C–H group is oriented into the pyridyl ring. This reflects a steric clash between *ortho* C–H groups on pairs of phenyl substituents in (*R*)-**3**, which is not present in its (*RS*)-isomer (Figure 3). The same ligand conformations are also adopted by other homo- and hetero-chiral $[M(L^{Ph})_2]^{2+}$ (M = Co,[32,49] Cu[50] or Zn[33]) complexes in the crystalline phase. In contrast, the isopropyl substituents in (*R*)-**4** exert a greater steric influence on the L^{iPr} ligand heterocyclic frameworks, but neighbouring pairs of *i*Pr groups are not in steric contact with each other (Figure 4).

The stability of the diastereomers of **3** and **4** in solution was probed by ^{1}H NMR. The paramagnetic NMR spectra of (*R*)-**3** and (*RS*)-**3** in CD_3CN are clearly distinguishable. Solutions of pre-isolated (*RS*)-**3** are clearly stable in this solvent, and contain no traces of homochiral (*R*)-**3** and (*S*)-**3** that would indicate the occurrence of ligand redistribution (Figure 5). For comparison, a freshly prepared 1:1:1 mixture of (*R*)-L^{Ph}, (*S*)-L^{Ph} and iron(II) salt does contain both diastereomers. That is consistent with a previous report that $\{Fe((R)\text{-}L^{Ph})[(S)\text{-}L^{Ph}]\}^{2+}$ exists as a single isomer with a diastereomeric excess of 0.95, as measured by mass spectrometry.[31]

In contrast, despite being phase-pure in the solid state, solutions of preformed (*RS*)-**4** in CD_3CN or $(CD_3)_2CO$ contain a mixture of (*R*)-**4**/(*S*)-**4** and (*RS*)-**4** by NMR (Figure 6).[40] The homochiral:heterochiral ratio in these solutions varies between about 1:5 and 1:3 in different spectra, becoming closer to the statistical 1:1 ratio upon standing for a period of hours. Hence, in contrast to (*RS*)-**3**, (*RS*)-**4** undergoes a degree of ligand redistribution in solution. These are the first such measurements on a $\{M((R)\text{-}L^{iPr})[(S)\text{-}L^{iPr}]\}^{2+}$ derivative.

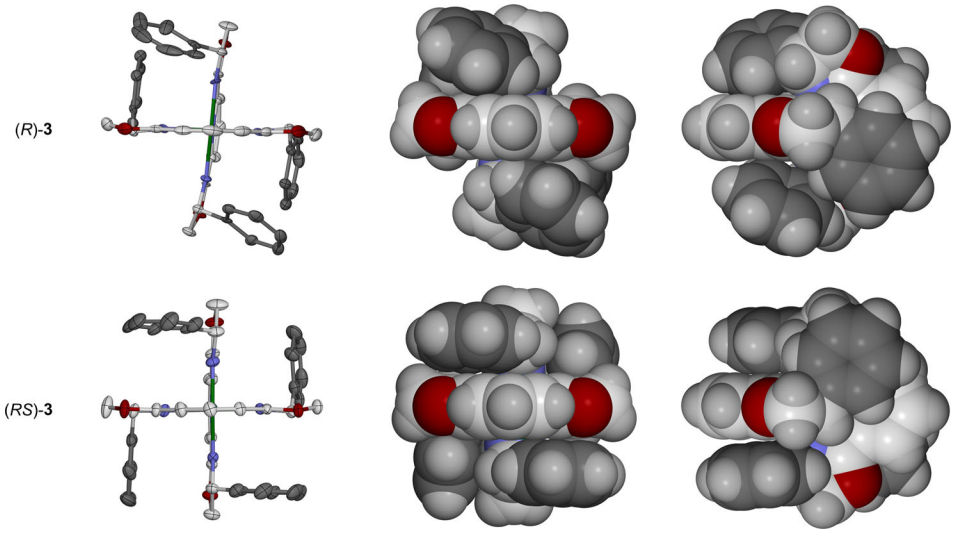

Figure 3. Structural comparison of the isomers of the $[Fe(L^{Ph})_2]^{2+}$ dication in (*R*)-**3**·$MeNO_2$ (phase 2, molecule A; top) and (*RS*)-**3**·3 MeCN (bottom). The left hand views have displacement ellipsoids at the 50% probability level, and H atoms omitted for clarity. The left and centre views are from the same orientation, whereas the right views are rotated by 90° to highlight steric contacts between ligand substituents in the homochiral isomer. Color code: C{heterocyclic}, white; C{phenyl}, dark gray; H, pale gray; Fe, green; N, blue; O, red.

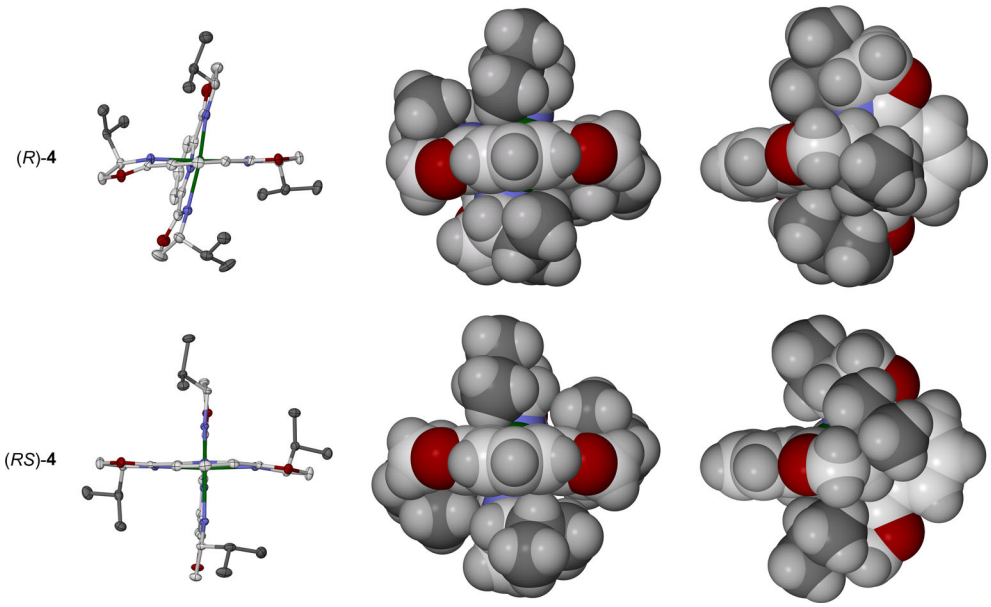

Figure 4. Structural comparison of the isomers of the $[Fe(L^{iPr})_2]^{2+}$ dication in (*R*)-**4**·$^1/_2$ MeCN (molecule A, top), and (*RS*)-**4** (bottom). Details are the same as those for Figure 3.

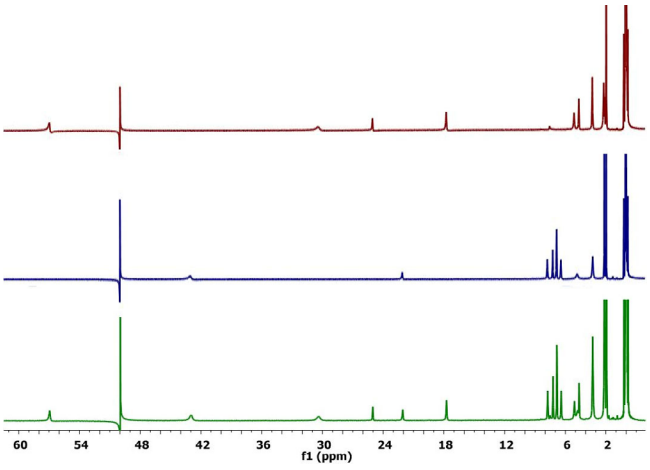

Figure 5. Paramagnetic NMR spectra in CD_3CN of: (*R*)-**3** (red, top); preformed (*RS*)-**3** (blue, middle); and, a 1:1:1 mixture of (*R*)-L^{Ph}, (*S*)-L^{Ph} and $Fe[ClO_4]_2$ (green, bottom). The feature at 50 ppm is a spectrometer artefact.

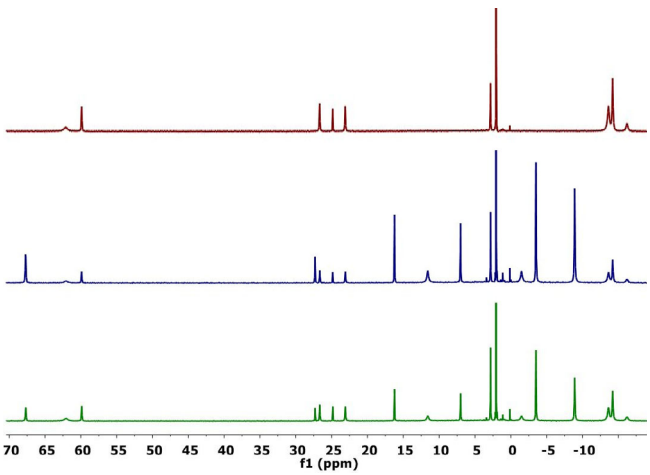

Figure 6. Paramagnetic NMR spectra in $(CD_3)_2CO$ of: (*R*)-**4** (red, top); preformed (*RS*)-**4** (blue, middle); and, a 1:1:1 mixture of (*R*)-L^{iPr}, (*S*)-L^{iPr} and $Fe[ClO_4]_2$ (green, bottom).

The spin states of all the complexes in solution were determined by variable temperature Evans method measurements (Figure 7 and Table 2).[51] The data were obtained in either CD_3CN or $(CD_3)_2CO$, according to the solubility of the compounds; the use of these different weakly polar solvents should have a minimal influence on the spin-state properties of the complexes.[52] Despite the ligand redistribution in solutions of (*RS*)-**4**, both isomers of **4** clearly remain fully high-spin between 186 and 322 K in $(CD_3)_2CO$. However, the other compounds all undergo thermal SCO under these conditions. The stability of their high-spin state relative to the low-spin state follows the order (Table 2): (*RS*)-**3** < (*R*)-**3** ≈ **1** < (*R*)-**2** ≪ (*R*)-**4**/(*RS*)-**4**.

The most important result is that the SCO $T_{1/2}$ is measurably lower in (*R*)-**3** than in (*RS*)-**3**. That is, the high-spin state of (*R*)-**3** is stabilized compared to (*RS*)-**3** under the same conditions. Although the difference is small, it is consistent with the more twisted coordination geometry adopted by (*R*)-**3** (Figure 3), which will disfavour the low-spin state as previously discussed.[43–47] The lower magnetic moment of (*RS*)-**3** at room temperature ($\chi_M T = 2.25\ cm^3\,mol^{-1}\,K$ at 293 K) compared to (*R*)-**3** ($3.12\ cm^3\,mol^{-1}\,K$) is also reflected in the reduced contact shifts in the NMR spectrum of (*RS*)-**3** (Figure 5).

More generally, the high-spin structure in both isomers of **4** will be sterically imposed, by the bulky *i*Pr substituents. This resembles analogous iron(II) complexes from the $[Fe(bpp)_2]^{2+}$ (bpp = 2,6-di{pyrazolyl}pyridine) series with distal isopropyl substituents, which are also exclusively high-spin.[48] In other respects, however, this trend does not mirror the steric proper-

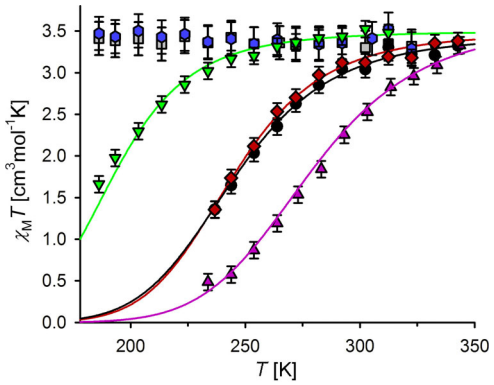

Figure 7. Solution-phase magnetic susceptibility data for: **1** (black circles); (*R*)-**2** (green triangles); (*R*)-**3** (red diamonds); (*RS*)-**3** (pink triangles); (*R*)-**4** (grey squares); (*RS*)-**4** (blue hexagons). The curves show the fits of the SCO equilibria to derive the thermodynamic parameters in Table 2.

Table 2. Solution-phase spin-crossover parameters for the compounds in this work (Figure 7).

	Solvent	$T_{1/2}$ [K]	ΔH [kJ mol^{-1}]	ΔS [J mol^{-1} K]
1	CD_3CN	245(2)	23.3	95
(*R*)-**2**	$(CD_3)_2CO$	192(2)	18.2	95
(*R*)-**3**	CD_3CN	244(2)	25.0	102
(*RS*)-**3**	CD_3CN	278(2)	26.2	94
(*R*)-**4**	$(CD_3)_2CO$	HS[a]	–	–
(*RS*)-**4**	$(CD_3)_2CO$	HS[a]	–	–

[a] HS = high-spin at all temperatures measured.

ties of the PyBox ligand substituents because $T_{1/2}$ for (*R*)-**2** is significantly lower than for **1** even though the methyl substituents in (*R*)-**2** have no steric influence on the metal coordination sphere.[40] Evidently, the inductive properties of the ligand substituents also influence the spin states of the $[Fe(L^R)_2]^{2+}$ centres. Electron-donating methyl substituents could reduce Fe→L^R backbonding into the oxazolinyl rings, which would weaken the ligand field and favour the high-spin state as observed. A comparable influence of ligand substituents on Fe→ligand π-bonding has also been seen in the $[Fe(bpp)_2]^{2+}$ series of complexes.[27]

Conclusion

The influence of chirality on the spin states of homochiral and heterochiral diastereomers of $[Fe(PyBox)_2]^{2+}$ derivatives has been investigated. As has been noted for other $[M(L^{Ph})_2]^{2+}$ complexes (M = Co, Cu and Zn),[32,33,49,50] (*R*)-**3** and (*R*)-**4** adopt more distorted coordination geometries than (*RS*)-**3** and (*RS*)-**4**, which reflects a significant twisting of the ligand conformations in the homochiral isomers. Although this is sterically imposed, the precise origin of the effect is different in the two compounds. In (*R*)-**3**, it reflects steric clashes between pairs of phenyl substituents, which force two phenyl groups to twist into the pyridyl ring of the other ligand in the molecule (Figure 3). In contrast the isopropyl groups in (*R*)-**4** are not in contact with each other, but have a much greater steric influence on the heterocyclic backbone of the co-ligand in the molecule (Figure 4).

The (*R*)-**3**/(*RS*)-**3** and (*R*)-**4**/(*RS*)-**4** isomer pairs each exhibit comparable spin-state properties; SCO-active for **3**, and high-spin for **4**. Moreover, the SCO $T_{1/2}$ temperatures for (*R*)-**3** and (*RS*)-**3** in the solid state are similarly above room temperature. Hence, the most important determinant of the spin-state properties of **1**–**4** in the solid state and in solution is evidently the identity of the ligand substituents. However, solution measurements, which are a more sensitive probe of the molecular ligand field, show a small stabilization of the high-spin state in (*R*)-**3** compared to (*RS*)-**3**. This is consistent with the sterically imposed, twisted ligand conformation in (*R*)-**3** (Figure 3), which favours the more structurally flexible high-spin form in complexes with this ligand geometry.[43–47] This is the first unambiguous demonstration of an influence of chirality on the spin state of an SCO complex. Our current work is aimed at computational ligand design and synthesis to enhance these effects, which have implications for chiral sensing using SCO reporter groups,[53] and for asymmetric catalysis.[6]

The optical purity of (*R*)- versus (*RS*)-$[M(L^{Ph})_2]^{2+}$ derivatives in solution has been investigated before,[31–33] but (*R*)- versus (*RS*)-$[M(L^{iPr})_2]^{2+}$ has not. It was unexpected that (*RS*)-**4** undergoes significant racemization through ligand redistribution in solution (Figure 6), whereas (*RS*)-**3** does not (Figure 5). The larger cone angle of the isopropyl substituents in **4** might have been expected to lead to a greater chiral discrimination in that compound, but clearly that is not the case. Steric contacts between the ligand substituents, which are more pronounced in (*R*)-**3** (Figure 3), may be more important in destabilizing the (*R*)-**3** isomer than the more general steric influence of the isopropyl groups in (*R*)-**4**.

Lastly, we have also described a gradual solid-state SCO transition in (*R*)-**3**·$MeNO_2$, with an unusual discontinuity below $T_{1/2}$ that is unconnected to a crystallographic phase change occurring at lower temperature (Figure 1). The origins of the discontinuity at 240 K are subtle, but correlate with the onset of whole molecule disorder below that temperature which becomes more pronounced upon further cooling to 190 K (Figure 2). Thermal contraction of the crystal lattice may occur more gradually than the SCO transition over this temperature range, affording a low-spin cation that is more compact than its lattice site. That would explain the unusual observation of increased molecular disorder at lower temperatures in this material.

Experimental Section

Instrumentation: Elemental microanalyses were performed by the microanalytical services in the University of Leeds, School of Chemistry, or the London Metropolitan University, School of Human Sciences. ^{1}H NMR spectra were obtained using Bruker DPX300 or Avance 500 FT spectrometers, operating at 300.2 and 500.1 MHz, respectively. X-ray powder diffraction data were obtained with a Bruker D8 Advance A25 diffractometer, using Cu-K_α radiation (λ = 1.5418 Å). Magnetic susceptibility measurements

were performed on a Quantum Design VSM SQUID magnetometer, in an applied field of 5000 G and a temperature ramp of 5 K min^{-1}. The samples were measured as freshly isolated polycrystalline materials, sealed inside air-tight VSM sample holder capsules. Where relevant, a drop of mother liquor was also added to the capsule to inhibit solvent loss during measurement. Diamagnetic corrections for the samples were estimated from Pascal's constants;[54] a previously measured diamagnetic correction for the sample holder was also applied to the data. Susceptibility measurements in solution were obtained by Evans method using a Bruker Avance 500 FT spectrometer operating at 500.13 MHz.[51] A diamagnetic correction for the sample,[54] and a correction for the variation of the density of the CD_3CN or $(CD_3)_2CO$ solvent with temperature,[55] were applied to these data. Thermodynamic parameters and spin-crossover midpoint temperatures were derived by fitting these data to Equations (1) and (2), in which *n*HS(*T*) is the high-spin fraction of the sample at temperature *T*:

$$\ln[(1-n\mathrm{HS}(T))/n\mathrm{HS}(T)] = \Delta H/RT - \Delta S/R \quad (1)$$

$$\Delta S = \Delta H/T_{1/2} \quad (2)$$

Materials and methods: Ligands 2,6-*bis*(oxazolinyl)pyridine (L^{H}) and 2,6-*bis*(4-(*R*)-methyloxazolinyl)pyridine ((*R*)-L^{Me}),[56] and the complex $[Fe(L^{H})_2][ClO_4]_2$,[35] were synthesized according to the literature procedures. All other reagents were purchased commercially and used as supplied, unless otherwise stated. **CAUTION!** Although we have experienced no problems in handling the compounds in this study, metal–organic perchlorates are potentially explosive and should be handled with due care in small quantities.

Synthesis of {Fe[(*R*)-L^{Me}]$_2$}[ClO_4]$_2$ [(*R*)-2]: Filtered solutions of $Fe[ClO_4]_2{\cdot}6H_2O$ (0.073 g, 0.20 mmol) and (*R*)-L^{Me} (0.10 g, 0.41 mmol) in nitromethane (25 cm^3) were mixed at room temperature, leading to an immediate dark red coloration. The solution was concentrated, and the product precipitated by addition of excess diethyl ether. Slow diffusion of diethyl ether vapour into a concentrated acetonitrile solution of the complex afforded large red blocks suitable for crystallographic characterization. Yield 0.15 g, 68 %. ^{1}H NMR (CD_3CN) $\delta = 2.2$ (12 H, CH_3), 11.6 (4 H, Ox H^3), 13.5 (4 H, Ox H^3), 24.8 (4 H, Ox H^4), 30.1 (2 H, Py H^4), 65.4 (4 H, Py $H^{3/5}$); elemental analysis calcd (%) for $C_{26}H_{30}Cl_2FeN_6O_{12}$ C 41.90, H 4.06, N 11.28; found C 42.02, H 4.04, N 11.25.

Synthesis of {Fe[(*R*)-L^{Ph}]$_2$}[ClO_4]$_2$ [(*R*)-3]: Addition of solid $Fe[ClO_4]_2{\cdot}6H_2O$ (0.040 g, 0.14 mmol) to a solution of (*R*)-L^{Ph} (0.10 g, 0.27 mmol) in acetonitrile (30 cm^3) afforded a dark purple mixture, which was stirred at room temperature until all the solid had dissolved. The solution was filtered and concentrated, and subsequent addition of excess diethyl ether yielded a dark purple powder. This was recrystallized from nitromethane by slow diffusion of diethyl ether vapour into a concentrated solution of the compound in nitromethane, to give purple crystals of the nitromethane solvate that lose their lattice solvent upon drying in vacuo. Yield 0.070 g, 52 %.^{1}H NMR (CD_3CN): $\delta = -3.1$ (8 H), 3.3 (8 H) (Ph $H^{2/6}$ + $H^{3/5}$), 4.7 (4 H), 5.1 (4 H) (Ox H^3 and Ph H^4), 17.8 (4 H, Ox H^3), 25.0 (2 H, Py H^4), 30.4 (4 H, Ox H^4), 57.0 (4 H, Py $H^{3/5}$); elemental analysis calcd (%) for $C_{46}H_{38}Cl_2FeN_6O_{12}$ C 55.61, H 3.86, N 8.46; found C 55.59, H 3.75, N 8.43.

Synthesis of {Fe[(*R*)-L^{Ph}][(*S*)-L^{Ph}]}[ClO_4]$_2$ [(*RS*)-3]: Method as for (*R*)-**3**, but using a mixture of (*R*)-L^{Ph} (0.05 g, 0.14 mmol) and (*S*)-L^{Ph} (0.05 g, 0.14 mmol). The crude product was recrystallized from acetonitrile/diethyl ether by the vapour diffusion method. Yield 0.18 g, 87 %. ^{1}H NMR (CD_3CN): $\delta = 3.3$ (8 H), 6.4 (8 H) (Ph $H^{2/6}$ + $H^{3/5}$), 4.8 (4 H), 6.9 (4 H), 7.2 (4 H), 7.8 (4 H) (Ox H^3 + H^4 and Ph H^4), 22.1 (2 H, Py H^4), 43.0 (4 H, Py $H^{3/5}$). elemental analysis calcd (%) for $C_{46}H_{38}Cl_2FeN_6O_{12}$ C 55.61, H 3.86, N 8.46; found 55.52, H 3.95, N 8.45.

Synthesis of {Fe[(*R*)-L^{iPr}]$_2$}[ClO_4]$_2$ [(*R*)-4]: Method as for (*R*)-**3**, using (*R*)-L^{iPr} (0.10 g, 0.33 mmol) and $Fe[ClO_4]_2{\cdot}6H_2O$ (0.060 g, 0.17 mmol). The product (*R*)-**4** is a wine-red solid, which was recrystallized as above from acetonitrile/diethyl ether. Yield 0.095 g, 87 %. ^{1}H NMR [$(CD_3)_2CO$] $\delta = -16.2$ (4 H, CH(CH_3)$_2$), -14.2 (12 H, CH(CH_3)$_2$), and -13.6 (12 H, CH(CH_3)$_2$), 23.1 (4 H), 24.9 (4 H), 26.7 (4 H), (Ox H^3 + H^4), 59.9 (4 H, Py $H^{3/5}$), 62.1 (2 H, Py H^4); elemental analysis calcd (%) for $C_{34}H_{46}Cl_2FeN_6O_{12}$ C 47.62, H 5.41, N 9.80; found C 47.57, H 5.38, N 9.86.

Synthesis of {Fe[(*R*)-L^{iPr}][(*S*)-L^{iPr}]}[ClO_4]$_2$ [(*RS*)-4]: Method as for (*R*)-**4**, but using a mixture of (*R*)-L^{iPr} (0.05 g, 0.17 mmol) and (*S*)-L^{iPr} (0.05 g, 0.17 mmol). The red solid complex forms solvent-free crystals from acetonitrile/diethyl ether. ^{1}H NMR [$(CD_3)_2CO$] $\delta = -8.9$ (12 H, CH(CH_3)$_2$), -3.5 (12 H, CH(CH_3)$_2$), -1.5 (4 H, CH(CH_3)$_2$), 7.0 (4 H), 11.6 (4 H), 16.2 (4 H) (Ox H^3 + H^4), 27.3 (2 H, Py H^4), 67.7 (4 H, Py $H^{3/5}$); peaks from homochiral (*R*)-**4**/(*S*)-**4** are also present in this spectrum (Figure 6); elemental analysis calcd (%) for $C_{34}H_{46}Cl_2FeN_6O_{12}$ C 47.62, H 5.41, N 9.80; found C 47.70, H 5.40, N 9.97.

Single-crystal structure analyses: Single crystals of the complexes were obtained as described above. All diffraction data were collected with an Agilent Supernova dual-source diffractometer using monochromated Cu-K_α radiation ($\lambda = 1.54184$ Å). The diffractometer is fitted with an Oxford Cryostream low-temperature device. All the structures were solved by direct methods (*SHELXS97*[57]), and developed by full least-squares refinement on F^2 (*SHELXL97*[57]). Crystallographic figures were prepared using *XSEED*,[58] whereas coordination volumes (V_{Oh}) were calculated using *Olex2*.[59] Experimental data from the structure determinations and descriptions of the crystallographic refinements are included in the Supporting Information.[40]

CCDC 1519275–1519290 and 1532884–1532890 contain the supplementary crystallographic data for this paper. These data are provided free of charge by The Cambridge Crystallographic Data Centre.

Acknowledgements

This work was funded by the Leverhulme Trust (RPG-2015-095), the EPSRC (EP/K012568/1 and EP/K00512X/1) and the University of Leeds. Support by COST network CM1305 *Explicit Control of Spin States in Technology and Biology (ECOSTBio)* is also acknowledged.

Conflict of interest

The authors declare no conflict of interest.

Keywords: chirality · iron · isomers · N-ligands · spin-crossover

[1] A. H. Ewald, R. L. Martin, G. Ross, A. H. White, *Proc. R. Soc. London Ser. A* **1964**, *280*, 235 – 257.
[2] P. Gütlich, H. A. Goodwin, *Top. Curr. Chem.* **2004**, 233 – 235.
[3] *Spin-Crossover Materials: Properties and Applications* (Ed.: M. A. Halcrow), Wiley, Chichester, **2013**, pp. 568.
[4] For other recent general reviews of SCO chemistry see: a) A. Bousseksou, G. Molnár, L. Salmon, W. Nicolazzi, *Chem. Soc. Rev.* **2011**, *40*, 3313 –

3335; b) P. Gütlich, *Eur. J. Inorg. Chem.* **2013**, 581 – 591; c) P. Gütlich, A. B. Gaspar, Y. Garcia, *Beilstein J. Org. Chem.* **2013**, *9*, 342 – 391; d) P. Guionneau, *Dalton Trans.* **2014**, *43*, 382 – 393; e) S. Brooker, *Chem. Soc. Rev.* **2015**, *44*, 2880 – 2892; f) O. Sato, *Nat. Chem.* **2016**, *8*, 644 – 656.

[5] M. A. Halcrow, *Chem. Soc. Rev.* **2011**, *40*, 4119 – 4142.

[6] *Spin States in Biochemistry and Inorganic Chemistry: Influence on Structure and Reactivity* (Eds.: M. Swart, M. Costas), Wiley, Chichester, **2016**, pp. 465.

[7] a) J. N. Harvey, R. Poli, K. M. Smith, *Coord. Chem. Rev.* **2003**, *238 – 239*, 347 – 361; b) S. Ye, C.-Y. Geng, S. Shaik, F. Neese, *Phys. Chem. Chem. Phys.* **2013**, *15*, 8017 – 8030; c) W. Nam, Y.-M. Lee, S. Fukuzumi, *Acc. Chem. Res.* **2014**, *47*, 1146 – 1154.

[8] P. L. Holland, *Acc. Chem. Res.* **2015**, *48*, 1696 – 1702.

[9] a) R. Bertoni, M. Lorenc, A. Tissot, M.-L. Boillot, E. Collet, *Coord. Chem. Rev.* **2015**, *282 – 283*, 66 – 76; b) R. Bertoni, M. Cammarata, M. Lorenc, S. F. Matar, J.-F. Létard, H. T. Lemke, E. Collet, *Acc. Chem. Res.* **2015**, *48*, 774 – 781.

[10] a) M. Matsuda, H. Tajima, *Chem. Lett.* **2007**, *36*, 700 – 701; b) K. Takahashi, H.-B. Cui, Y. Okano, H. Kobayashi, H. Mori, H. Tajima, Y. Einaga, O. Sato, *J. Am. Chem. Soc.* **2008**, *130*, 6688 – 6689; c) A. Rotaru, I. A. Gural'skiy, G. Molnár, L. Salmon, P. Demont, A. Bousseksou, *Chem. Commun.* **2012**, *48*, 4163 – 4165; d) H. Phan, S. M. Benjamin, E. Steven, J. S. Brooks, M. Shatruk, *Angew. Chem. Int. Ed.* **2015**, *54*, 823 – 827; *Angew. Chem.* **2015**, *127*, 837 – 841; e) Yu. N. Shvachko, D. V. Starichenko, A. V. Korolyov, E. B. Yagubskii, A. I. Kotov, L. I. Buravov, K. A. Lyssenko, V. N. Zverev, S. V. Simonov, L. V. Zorina, O. G. Shakirova, L. G. Lavrenova, *Inorg. Chem.* **2016**, *55*, 9121 – 9130.

[11] a) Y. Garcia, F. Robert, A. D. Naik, G. Zhou, B. Tinant, K. Robeyns, S. Michotte, L. Piraux, *J. Am. Chem. Soc.* **2011**, *133*, 15850 – 15853; b) S. Titos-Padilla, J. M. Herrera, X.-W. Chen, J. J. Delgado, E. Colacio, *Angew. Chem. Int. Ed.* **2011**, *50*, 3290 – 3293; *Angew. Chem.* **2011**, *123*, 3348 – 3351; c) C.-F. Wang, R.-F. Li, X.-Y. Chen, R.-J. Wei, L.-S. Zheng, J. Tao, *Angew. Chem. Int. Ed.* **2015**, *54*, 1574 – 1577; *Angew. Chem.* **2015**, *127*, 1594 – 1597; d) J. M. Herrera, S. Titos-Padilla, S. J. A. Pope, I. Berlanga, F. Zamora, J. J. Delgado, K. V. Kamenev, X. Wang, A. Prescimone, E. K. Brechin, E. Colacio, *J. Mater. Chem. C* **2015**, *3*, 7819 – 7829; e) J.-L. Wang, Q. Liu, X.-J. Lv, R.-L. Wang, C.-Y. Duan, T. Liu, *Dalton Trans.* **2016**, *45*, 18552 – 18558.

[12] a) Z.-P. Ni, J.-L. Liu, M. N. Hoque, W. Liu, J.-Y. Li, Y.-C. Chen, M.-L. Tong, *Coord. Chem. Rev.* **2017**, *335*, 28 – 43; b) R. Ohtani, S. Hayami, *Chem. Eur. J.* **2017**, *23*, 2236 – 2248.

[13] a) O. Kahn, C. J. Martinez, *Science* **1998**, *279*, 44 – 48; b) C. Lefter, S. Rat, J. S. Costa, M. D. Manrique-Juárez, C. M. Quintero, L. Salmon, I. Séguy, T. Leichle, L. Nicu, P. Demont, A. Rotaru, G. Molnár, A. Bousseksou, *Adv. Mater.* **2016**, *28*, 7508 – 7514; c) M. D. Manrique-Juárez, S. Rat, L. Salmon, G. Molnár, C. M. Quintero, L. Nicu, H. J. Shepherd, A. Bousseksou, *Coord. Chem. Rev.* **2016**, *308*, 395 – 408.

[14] a) M. Cavallini, *Phys. Chem. Chem. Phys.* **2012**, *14*, 11867 – 11876; b) H. J. Shepherd, G. Molnár, W. Nicolazzi, L. Salmon, A. Bousseksou, *Eur. J. Inorg. Chem.* **2013**, 653 – 661; c) A. Tissot, *New J. Chem.* **2014**, *38*, 1840 – 1845; d) C. Lefter, V. Davesne, L. Salmon, G. Molnár, P. Demont, A. Rotaru, A. Bousseksou, *Magnetochemistry* **2016**, *2*, 18.

[15] a) G. D. Harzmann, R. Frisenda, H. S. J. van der Zant, M. Mayor, *Angew. Chem. Int. Ed.* **2015**, *54*, 13425 – 13430; *Angew. Chem.* **2015**, *127*, 13624 – 13630; b) A. C. Aragonès, D. Aravena, J. I. Cerdá, Z. Acís-Castillo, H. Li, J. A. Real, F. Sanz, J. Hihath, E. Ruiz, I. Díez-Pérez, *Nano Lett.* **2016**, *16*, 218 – 226.

[16] P. G. Lacroix, I. Malfant, J.-A. Real, V. Rodriguez, *Eur. J. Inorg. Chem.* **2013**, 615 – 627.

[17] S. Ohkoshi, S. Takano, K. Imoto, M. Yoshikiyo, A. Namai, H. Tokoro, *Nat. Photonics* **2013**, *8*, 65 – 71.

[18] a) M. Clemente-León, E. Coronado, C. Martí-Gastaldo, F. M. Romero, *Chem. Soc. Rev.* **2011**, *40*, 473 – 497; b) Y. Sunatsuki, S. Miyahara, Y. Sasaki, T. Suzuki, M. Kojima, N. Matsumoto, *CrystEngComm* **2012**, *14*, 6377 – 6380; c) M. Clemente-León, E. Coronado, M. López-Jordà, J. C. Waerenborgh, C. Desplanches, H. Wang, J.-F. Létard, A. Hauser, A. Tissot, *J. Am. Chem. Soc.* **2013**, *135*, 8655 – 8667; d) M. López-Jordà, M. Giménez-Marqués, C. Desplanches, G. M. Espallargas, M. Clemente-León, E. Coronado, *Eur. J. Inorg. Chem.* **2016**, 2187 – 2192.

[19] I. A. Gural'skiy, O. I. Kucheriv, S. I. Shylin, V. Ksenofontov, R. A. Polunin, I. O. Fritsky, *Chem. Eur. J.* **2015**, *21*, 18076 – 18079; I. A. Gural'skiy, V. A. Reshetnikov, A. Szebesczyk, E. Gumienna-Kontecka, A. I. Marynin, S. I. Shylin, V. Ksenofontov, I. O. Fritsky, *J. Mater. Chem. C* **2015**, *3*, 4737 – 4741.

[20] a) S. E. Howson, L. E. N. Allan, N. P. Chmel, G. J. Clarkson, R. J. Deeth, A. D. Faulkner, D. H. Simpson, P. Scott, *Dalton Trans.* **2011**, *40*, 10416 – 10433; b) T. Hashibe, T. Fujinam, D. Furusho, N. Matsumoto, Y. Sunatsuki, *Inorg. Chim. Acta* **2011**, *375*, 338 – 342.

[21] a) Z.-G. Gu, C.-Y. Pang, D. Qiu, J. Zhang, J.-L. Huang, L.-F. Qin, A.-Q. Sun, Z. Li, *Inorg. Chem. Commun.* **2013**, *35*, 164 – 168; b) D.-H. Ren, X.-L. Sun, L. Gu, D. Qiu, Z. Li, Z.-G. Gu, *Inorg. Chem. Commun.* **2015**, *51*, 50 – 54; c) D.-H. Ren, D. Qiu, C.-Y. Pang, Z. Li, Z.-G. Gu, *Chem. Commun.* **2015**, *51*, 788 – 791.

[22] L.-F. Qin, C.-Y. Pang, W.-K. Han, F.-L. Zhang, L. Tian, Z.-G. Gu, X. Ren, Z. Li, *CrystEngComm* **2015**, *17*, 7956 – 7963.

[23] L.-F. Qin, C.-Y. Pang, W.-K. Han, F.-L. Zhang, L. Tian, Z.-G. Gu, X. Ren, Z. Li, *Dalton Trans.* **2016**, *45*, 7340 – 7348.

[24] R. T. Acha, M. Pilkington, *CrystEngComm* **2015**, *17*, 8897 – 8905.

[25] Q. Wang, S. Venneri, N. Zarrabi, H. Wang, C. Desplanches, J.-F. Létard, T. Seda, M. Pilkington, *Dalton Trans.* **2015**, *44*, 6711 – 6714.

[26] Y. Sekimoto, M. R. Karim, N. Saigo, R. Ohtani, M. Nakamura, S. Hayami, *Eur. J. Inorg. Chem.* **2017**, 1049 – 1053.

[27] L. J. Kershaw Cook, R. Kulmaczewski, R. Mohammed, S. Dudley, S. A. Barrett, M. A. Little, R. J. Deeth, M. A. Halcrow, *Angew. Chem. Int. Ed.* **2016**, *55*, 4327 – 4331; *Angew. Chem.* **2016**, *128*, 4399 – 4403.

[28] G. Desimoni, G. Faita, P. Quadrelli, *Chem. Rev.* **2003**, *103*, 3119 – 3154.

[29] a) J. S. Johnson, D. A. Evans, *Acc. Chem. Res.* **2000**, *33*, 325 – 335; b) H. C. Aspinall, N. Greeves, *J. Organomet. Chem.* **2002**, *647*, 151 – 157; c) S. Kobayashi, Y. Yamashita, *Acc. Chem. Res.* **2011**, *44*, 58 – 71; d) B. D. Ward, L. H. Gade, *Chem. Commun.* **2012**, *48*, 10587 – 10599.

[30] a) S. Chorazy, K. Nakabayashi, K. Imoto, J. Mlynarski, B. Sieklucka, S. Ohkoshi, *J. Am. Chem. Soc.* **2012**, *134*, 16151 – 16154; b) S. Chorazy, K. Nakabayashi, N. Ozaki, R. Pelka, T. Fic, J. Mlynarski, B. Sieklucka, S. Ohkoshi, *RSC Adv.* **2013**, *3*, 1065 – 1068; c) S. Chorazy, K. Nakabayashi, M. Arczynski, R. Pelka, S. Ohkoshi, B. Sieklucka, *Chem. Eur. J.* **2014**, *20*, 7144 – 7159.

[31] H. Sato, Y. Suzuki, Y. Takai, H. Kawasaki, R. Arakawa, M. Shizuma, *Chem. Lett.* **2010**, *39*, 564 – 566.

[32] C. Provent, G. Bernardinelli, A. F. Williams, N. Vulliermet, *Eur. J. Inorg. Chem.* **2001**, 1963 – 1967.

[33] S. Saaby, K. Nakama, M. A. Lie, R. G. Hazell, K. A. Jørgensen, *Chem. Eur. J.* **2003**, *9*, 6145 – 6154.

[34] Y.-Y. Zhu, C.-W. Liu, J. Yin, Z.-S. Meng, Q. Yang, J. Wang, T. Liu, S. Gao, *Dalton Trans.* **2015**, *44*, 20906 – 20912.

[35] Y.-Y. Zhu, H.-Q. Li, Z.-Y. Ding, X.-J. Lu, L. Zhao, Y.-S. Meng, T. Liu, S. Gao, *Inorg. Chem. Front.* **2016**, *3*, 1624 – 1636.

[36] A second solvate of (*R*)-**3**, (*R*)-**3**·MeCN, was also examined during this work. This solvate suffers from twinning but has the same unit cell dimensions as Phase 1 of (*R*)-**3**·$MeNO_2$ at 120 K. Magnetic susceptibility data from (*R*)-**3**·MeCN show spin-crossover that is similar in form to (*R*)-**3**·$MeNO_2$ but shifted to lower temperature, including a clear discontinuity near 150 K. Further details are in the Supporting Information; see also ref. [40].

[37] See eg a) M. Yamada, M. Ooidemizu, Y. Ikuta, S. Osa, N. Matsumoto, S. Iijima, M. Kojima, F. Dahan, J.-P. Tuchagues, *Inorg. Chem.* **2003**, *42*, 8406 – 8416; b) B. Weber, C. Carbonera, C. Desplances, J.-F. Létard, *Eur. J. Inorg. Chem.* **2008**, 1589 – 1598; c) J. Tang, J. S. Costa, S. Smulders, G. Molnár, A. Bousseksou, S. J. Teat, Y. Li, G. A. van Albada, P. Gamez, J. Reedijk, *Inorg. Chem.* **2009**, *48*, 2128 – 2135.

[38] a) M. Shatruk, H. Phan, B. A. Chrisostomo, A. Suleimenova, *Coord. Chem. Rev.* **2015**, *289 – 290*, 62 – 73; b) N. Ortega-Villar, M. C. Muñoz, J. A. Real, *Magnetochemistry* **2016**, *2*, 16.

[39] a) V. A. Money, J. Elhaïk, I. R. Evans, M. A. Halcrow, J. A. K. Howard, *Dalton Trans.* **2004**, 65 – 69; b) G. S. Matouzenko, D. Luneau, G. Molnár, N. Ould-Moussa, S. Zein, S. A. Borshch, A. Bousseksou, F. Averseng, *Eur. J. Inorg. Chem.* **2006**, 2671 – 2682.

[40] The Supporting Information to this article contains crystallographic experimental data and refinement details; more detailed definitions of the structure parameters in Table 1 (see refs. [41, 42]; additional crystallographic Figures and Tables of metric parameters; variable temperature unit cell data for (*R*)-**3**·$MeNO_2$; and, solid state magnetic susceptibility and X-ray powder diffraction data.

[41] V_{Oh} is the volume of the FeN_6 coordination octahedron in the complex molecule, which is typically about 10 Å^3 in the low-spin state and 13 Å^3 in high-spin state of iron(II) complexes. Σ is a general measure of the deviation of a metal ion from an ideal octahedral geometry, whereas Θ more specifically indicates its distortion towards a trigonal prismatic structure. Both Σ and Θ are usually much larger in the high-spin than in the low-spin state; a perfectly octahedral complex gives $\Sigma = \Theta = 0$. Mathematical definitions of Σ and Θ are in the Supporting Information to this article. P. Guionneau, M. Marchivie, G. Bravic, J.-F. Létard, D. Chasseau, *Top. Curr. Chem.* **2004**, *234*, 97 – 128.

[42] θ is the dihedral angle between the least squares planes of the two L^R ligands, and ϕ is the *trans*-N{pyridyl}-Fe-N{pyridyl} bond angle (Scheme S1, Supporting Information) (ref. [42]). An ideal D_{2d}-symmeric geometry for $[Fe(PyBox)_2]^{2+}$ centres gives $\theta = 90$ and $\phi = 180^\circ$, but high-spin complexes with related *tris*-heterocyclic ligands often exhibit distorted structures with significantly reduced values for these parameters.[43]

[43] M. A. Halcrow, *Coord. Chem. Rev.* **2009**, *253*, 2493 – 2514.

[44] L. J. Kershaw Cook, R. Mohammed, G. Sherborne, T. D. Roberts, S. Alvarez, M. A. Halcrow, *Coord. Chem. Rev.* **2015**, *289 – 290*, 2 – 12.

[45] J. M. Holland, J. A. McAllister, C. A. Kilner, M. Thornton-Pett, A. J. Bridgeman, M. A. Halcrow, *J. Chem. Soc. Dalton Trans.* **2002**, 548 – 554.

[46] L. J. Kershaw Cook, F. L. Thorp-Greenwood, T. P. Comyn, O. Cespedes, G. Chastanet, M. A. Halcrow, *Inorg. Chem.* **2015**, *54*, 6319 – 6330.

[47] a) S. Vela, J. J. Novoa, J. Ribas-Arino, *Phys. Chem. Chem. Phys.* **2014**, *16*, 27012 – 27024; b) M. Fumanal, F. Jiménez-Grávalos, J. Ribas-Arino, S. Vela, *Inorg. Chem.* **2017**, *56*, 4474 – 4483.

[48] a) J. M. Holland, S. A. Barrett, C. A. Kilner, M. A. Halcrow, *Inorg. Chem. Commun.* **2002**, *5*, 328 – 332; b) T. D. Roberts, M. A. Little, L. J. Kershaw Cook, S. A. Barrett, F. Tuna, M. A. Halcrow, *Polyhedron* **2013**, *64*, 4 – 12.

[49] J. Guo, B. Wang, J. Bi, C. Zhang, H. Zhang, C. Bai, Y. Hu, X. Zhang, *Polymer* **2015**, *59*, 124 – 132.

[50] D. A. Evans, M. C. Kozlowski, J. A. Murry, C. S. Burgey, K. R. Campos, B. T. Connell, R. J. Staples, *J. Am. Chem. Soc.* **1999**, *121*, 669 – 685.

[51] a) D. F. Evans, *J. Chem. Soc.* **1959**, 2003 – 2005; b) E. M. Schubert, *J. Chem. Educ.* **1992**, *69*, 62.

[52] S. A. Barrett, C. A. Kilner, M. A. Halcrow, *Dalton Trans.* **2011**, *40*, 12021 – 12024.

[53] See *eg* a) Z. Ni, M. P. Shores, *J. Am. Chem. Soc.* **2009**, *131*, 32 – 33; b) M. C. Young, E. Liew, R. J. Hooley, *Chem. Commun.* **2014**, *50*, 5043 – 5045; c) M. Darawsheh, L. A. Barrios, O. Roubeau, S. J. Teat, G. Aromí, *Chem. Eur. J.* **2016**, *22*, 8635 – 8645.

[54] C. J. O'Connor, *Prog. Inorg. Chem.* **1982**, *29*, 203 – 283.

[55] a) W. A. Felsing, S. A. Durban, *J. Am. Chem. Soc.* **1926**, *48*, 2885 – 2893; b) H. Kratzke, S. Müller, *J. Chem. Thermodyn.* **1985**, *17*, 151 – 158; c) B. García, J. C. Ortega, *J. Chem. Eng. Data* **1988**, *33*, 200 – 204.

[56] M. K. Tse, S. Bhor, M. Klawonn, G. Anilkumar, H. Jiao, C. Döbler, A. Spannenberg, W. Mägerlein, H. Hugl, M. Beller, *Chem. Eur. J.* **2006**, *12*, 1855 – 1874.

[57] G. M. Sheldrick, *Acta Crystallogr. Sect. A* **2008**, *64*, 112 – 122.

[58] L. J. Barbour, *J. Supramol. Chem.* **2001**, *1*, 189 – 191.

[59] O. V. Dolomanov, L. J. Bourhis, R. J. Gildea, J. A. K. Howard, H. Puschmann, *J. Appl. Crystallogr.* **2009**, *42*, 339 – 341.

Manuscript received: February 21, 2017

Accepted Article published: April 7, 2017

Final Article published: ■■ ■■, 0000

FULL PAPER

Iron Complexes

*K. E. Burrows, S. E. McGrath, R. Kulmaczewski, O. Cespedes, S. A. Barrett, M. A. Halcrow**

■■ – ■■

Spin States of Homochiral and Heterochiral Isomers of $[Fe(PyBox)_2]^{2+}$ Derivatives

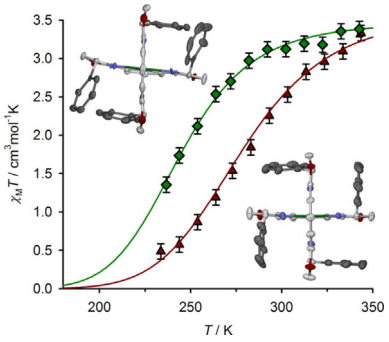

A heated switch: Homochiral $[Fe((R)\text{-}L^{Ph})_2]^{2+}$ (green; L^{Ph} = 2,6-*bis*{4-phenyloxazolinyl}pyridine) undergoes spin-crossover in CD_3CN at 34 K lower temperature than its heterochiral diastereomer $[Fe((R)\text{-}L^{Ph})((S)\text{-}L^{Ph})]^{2+}$ (red). This is attributed to a more twisted coordination geometry in the homochiral isomer, reflecting a steric clash between phenyl substituents. The equivalent diastereomers of $[Fe(L^{iPr})_2]^{2+}$ (L^{iPr} = 2,6-*bis*{4-isopropyloxazolinyl}pyridine) are both high-spin.